Proceedings of the ASME 2010 3rd Joint US-European Fluids Engineering Summer Meeting and 8th International Conference on Nanochannels, Microchannels, and Minichannels
FEDSM-ICNMM2010
August 1-5, 2010, Montreal, Canada

FEDSM-ICNMM2010-30804

QUASI-PERIODIC STRUCTURE OF VORTICAL FLOWS PRODUCED IN THE WAKE OF FINITE BLUFF BODIES PARTIALLY IMMERSED IN A BOUNDARY LAYER

Jason A. Bourgeois*
Department of Mechanical and Manufacturing Engineering
University of Calgary
Calgary, AB T2N 1N4
Canada
Email: jabourge@ucalgary.ca

Pooria Sattari
Robert J. Martinuzzi
Department of Mechanical and Manufacturing Engineering
University of Calgary
Calgary, AB T2N 1N4
Canada

ABSTRACT

The quasi-periodic vortex shedding structure in the wake of finite surface-mounted square- and circular-cross-section cylinders is investigated for several aspect ratios. Complex continuous wavelet transforms (CWT's) are used to obtain a phase function $\phi(t)$ from hot-wire measurements. Mean relative phases and phase averaged particle image velocimetry (PIV) measurements indicate an upstream bending of the initially vertical shed vortex structures for all obstacles investigated. This upstream bending mechanism reorients vorticity streamwise and is described in terms of Biot-Savart induction that occurs at the junction of the tip and side shear layers. This mechanism of vorticity concentration/reorientation is inherently three-dimensional and interacts with the nominally two-dimensional mechanism of alternate vortex sheet roll-up from the opposing obstacle side faces. This mechanism typically acts higher along the height for square- as opposed to circular-cross section cylinders and plays a more dominant role for smaller aspect ratios.

NOMENCLATURE

- d Width (hydraulic diameter) of cross-section.
- f Frequency.
- h Height of cylinder.
- Re Reynolds number.
- S_{ij} Strain-rate tensor.
- St Strouhal number.
- $\mathbf{u}$ Instantaneous velocity vector.
- $\mathbf{u}'$ Fluctuating velocity vector of the phase averaged velocity.
- $\mathbf{U}$ Phase averaged velocity vector.
- U_c Convective velocity.
- U_∞ Free stream velocity.
- $\mathbf{x}$ Position vector.
- x Streamwise coordinate.
- y Lateral coordinate.
- z Vertical coordinate.
- δ Boundary layer thickness.
- λ Wavelet scale.
- λ_2 Second eigenvalue of the tensor $S_{ij}S_{jk}+\Omega_{ij}\Omega_{jk}$.
- ν Kinematic viscosity.
- τ Wavelet time lag.
- ϕ Phase angle.
- Φ Power spectral density.
- ψ Wavelet function.
- $\boldsymbol{\omega}$ Instantaneous vorticity vector.
- $\boldsymbol{\omega}'$ Fluctuating vorticity vector of the phase averaged velocity.
- $\boldsymbol{\Omega}$ Phase averaged vorticity vector.
- Ω_{ij} Rotation-rate tensor.

*Address all correspondence to this author.

1 INTRODUCTION

Bluff body flows generally give rise to regions of separated flow from which vortical structures are shed. When the obstacles are surface mounted, these structures interact with the vorticity contained within the horseshoe vortex (formed at the obstacle–surface junction) and other streamwise vorticity (e.g., tip vortices) in the flow and lead to complex three-dimensional structure and dynamics. Of interest is the vortex structure when shedding is quasi-periodic. Changes between symmetric and anti-symmetric modes of the shedding topology with vertical position have been reported in the literature. However, conditions reported for these changes have not always been consistent [1, 2]. Moreover, several models depicting the vortex skeleton structure in the wake have been proposed. While these explain some phenomenological aspects, they are generally not fully consistent with topological principles. Solenoidality of the vorticity field in a homogeneous fluid requires that vortex lines form rings or terminate on the fluid boundaries and that vorticity is imparted to the flow only at the boundaries by the pressure gradient. As the vortex lines must in three-dimensions satisfy solenoidality and on the assumption that the correlated vortex structure will be determined by the vortex line topology, the structure at one vertical position is not independent of the structure at other positions.

In this work, the emphasis is placed on the streamwise reorientation of vortex structures generated initially with the vorticity axis normal to the flow. The emphasis herein will be that of streamwise reorientation of initially vertical vortices. Mean field streamwise free end and base vortex structures have been described by [3–6] but the mechanism of their generation has not been adequately explained. Previous observations have noted counter-rotating streamwise vortex pairs in the wake. The sense of rotation differs according to the obstacle shape (cross-sectional geometry and aspect ratio, h/d) and flow conditions (Re, boundary layer to height ratio δ/d, and turbulence intensity) causing in some cases upwash or, in others, downwash along the plane of symmetry in the wake.

Proposed models of the vortex structure typically address either the mean field structure or the instantaneous structure of a single shed vortex. However, mean structures arise from the averaging process and thus must arise from the passage of the shed vortices such that the mean and instantaneous flow fields must be consistent and satisfy topological constraints.

To elucidate the connectivity in the quasi-periodic vortex shedding process around finite bluff bodies immersed in a boundary layer, results of hot wire anemometry (HWA) and particle image velocimetry (PIV) measurements will be interpreted according to the solenoidality of the phase averaged wake. Square and circular section cylinders of aspect ratios h/d =1, 2, and 4 have been investigated for $Re \approx O(10^4)$. To distinguish the instantaneous vortex phase from the remaining energetic content at other scales, the continuous wavelet transform (CWT) of the measurement signal is taken using a complex Morlet wavelet at the frequency of the vortex shedding process.

The spatial distribution of relative phase at the shedding frequency is presented and the vortex topology is deduced. Observations of the shedding mode in the relative phase field indicate oblique angles of shedding along the height and the effects of aspect ratio and cross-sectional geometry. Proposed streamwise oriented free end and base vortex structures which have been argued to exist based on experimentally observed mean streamwise vorticity by [3–6] in fact are not in a phase averaged sense distinct from the shed vortices. In fact, observations of the phase field indicate that there is a tendency for the shed vortices to bend back towards the obstacle, consistent with arguments that can be made based on the Biot-Savart law and the initial spatial distribution of the shed vorticity.

2 EXPERIMENTAL FACILITY

Measurements were conducted in a 16:1-inlet-contraction open-test-section wind tunnel at the University of Calgary. The working section of the tunnel has a jet diameter of 0.5m in which a flat plate with a sharp leading edge is placed, as shown schematically in Fig. 1. Finite square- and circular-cross-section cylinders of aspect ratio h/d =1, 2, and 4 are mounted on the flat plate. The height of all obstacles is h =50.8mm, and the ratio of boundary layer thickness to obstacle height is held fixed.

The coordinate system is taken to have an origin at the centre of the obstacle on the plate surface, as in Fig. 1. The x-coordinate axis is taken as streamwise, the z-coordinate axis as the direction normal to the plate, and the y-coordinate axis as the lateral direction.

Measurements were taken at free-stream velocities of U_∞= 8 m/s and 15 m/s which correspond respectively to Reynolds numbers of $Re = Ud/\nu$ =26,000 and 48,000 for $h/d = 1$, Re =13,000 and 24,000 for $h/d = 2$, and Re =6,500 and 12,000 for $h/d = 4$. The free-stream turbulence intensity of the tunnel at the lower and higher Re is 0.6% and 0.3%. The boundary layer thickness at the mounting location of the finite cylinders with the cylinders removed is approximately $\delta/h \approx 0.3$ and 0.2, respectively. The Strouhal number, $St = fd/U_\infty$, for the shedding frequency (corresponding to the peak in the Fourier power spectrum) for the range of aspect ratios of square-cross-section cylinders at different measurement positions falls in the range $St = 0.09$ to $St = 0.11$. For circular cylinders, the Strouhal number ranges from $St = 0.13$ to $St = 0.15$.

Up to five hot-wire anemometers have been used simultaneously (TSI model 1210-20). One anemometer monitored the free-stream velocity, up to three anemometers would be used in a traversed vertical rake, and typically one would be used as a fixed phase reference. Anemometer sampling rates were 10.24 kHz. For the various obstacles and Reynolds numbers, this rate corresponds to approximately 60 to 700 data points per shedding cycle. An anti-aliasing filter was used at 5kHz. The histogram for

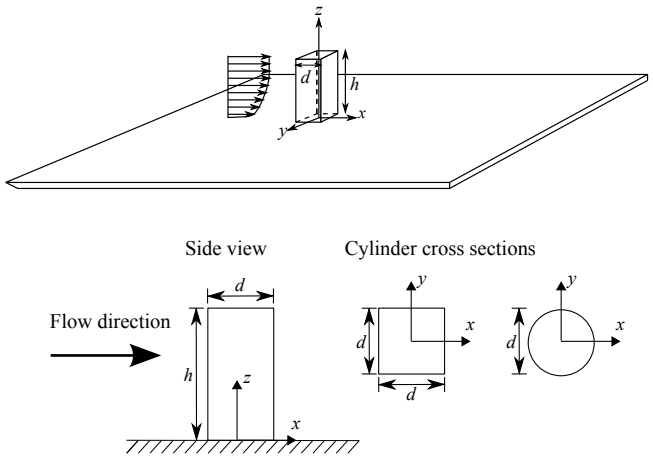

FIGURE 1: SCHEMATIC OF OBSTACLE AND PLATE USED TO GENERATE THE FLOW.

the velocity was monitored at each measurement point to ensure that a rectified-signal bias (i.e., misinterpretation due to negative velocity) did not occur.

High-frame-rate PIV (using a LaVision FlowMaster high-speed system) was conducted at various horizontal planes in the wake of a $h/d = 4$ square cylinder. Frame rates of 0.5 and 1 kHz have being used, corresponding to approximately 5 to 10 data points per shedding cycle. The PIV-system cameras provided for 1024×1024 pixel resolution. The system was operated in double-pulse mode (with a pulse separation of 50μs). Interrogation windows, using 32×32 pixels in a frame straddled arrangement, resulted in a spatial resolution of 3mm. The surface pressure was measured at a height of $0.25h$ (where the fluctuation magnitude of hot-wire measurements is typically very strong) in order to have a fixed reference for the phase of the vortex shedding process. Pressure sampling rates were 10.24 kHz—the same sampling rate as the hot wires—and were sychronized with the PIV measurements using a TTL trigger sent from the PIV system at the start of a measurement.

3 METHODOLOGY OF PHASE ANALYSIS

The frequency peak of the power spectrum of wake measurements has no identifiable variation in space. If it is to be assumed that the wake is made up of convecting coherent vortex structures, it should be verified that the convective velocity similarly lacks spatial variation downstream of the formation region. Cross-correlating phase averaged measurements at subsequent points with known separation along the streamwise direction, the time lag of maximum correlation at the two points can be used to obtain the convective velocity. A lateral average convective velocity is shown in Fig. 2 for three vertical positions in the wake for x/d ranging from 2 to 11. The convective velocity is constant along the height and becomes approximately constant at $U_c \approx 0.75U_\infty$ along the streamwise direction after approximately six diameters. With a constant convective velocity and frequency in the wake, the field can properly be analysed according to the phases of the fluctuations at the shedding frequency.

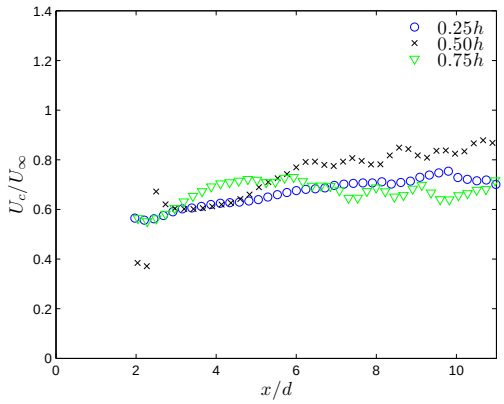

FIGURE 2: CALCULATED CONVECTIVE VELOCITY AT THREE PLANES FROM PIV MEASUREMENTS.

In order to properly exploit the quasi-periodic nature of the flow when building meaningful statistics, a suitable phase-determination methodology must be used. Quasi-periodicity of the flow means that the primary energetic mode of the flow repeats, having a certain amount of stochastic variability of the period and the field variables. The pronounced peak in the Fourier power spectrum of velocity measurements, as in Fig. 3, clearly indicates that the analyzed wakes are indeed quasi-periodic. This pronounced peak is found in the wake of aspect ratio $h/d = 1$, 2, and 4 square cylinders and $h/d = 2$ and 4 circular cylinders. The peak is absent in the power spectrum of the $h/d = 1$ circular cylinder, consistent with the work of [1].

The instantaneous flow variables of a quasi-periodic flow can be decomposed as the sum of a coherent (phase averaged) part and an incoherent (random) part. For the velocity and vorticity, these are

$$\mathbf{u}(\mathbf{x},\phi_R(t),t) = \mathbf{U}(\mathbf{x},\phi_R(t)) + \mathbf{u}'(\mathbf{x},t) \tag{1}$$

where $\phi_R(t)$ is a given phase reference of the shedding cycle and

$$\boldsymbol{\omega}(\mathbf{x},\phi_R(t),t) = \boldsymbol{\Omega}(\mathbf{x},\phi_R(t)) + \boldsymbol{\omega}'(\mathbf{x},t) \tag{2}$$

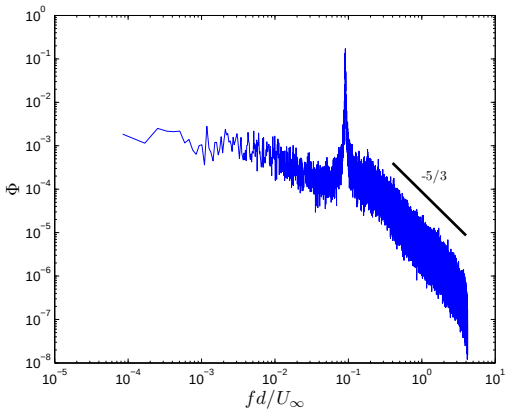

FIGURE 3: POWER SPECTRUM OF A HOT-WIRE VELOCITY SIGNAL COLLECTED AT $x/d = 3$, $y/d = 2$, AND $z/h = 0.5$ FOR A $h/d = 4$ SQUARE-CROSS-SECTION CYLINDER.

As averaging and differentiation are both linear operations, the solenoidality condition on the instantaneous velocity and vorticity fields result in the average fields obeying the solenoidality condition as well, $\nabla \cdot \mathbf{U} = 0$ and $\nabla \cdot \boldsymbol{\Omega} = 0$. The solenoidality of the fluctuations is ensured by the difference of the instantaneous and averaged solenoidal conditions, $\nabla \cdot \mathbf{u}' = 0$ and $\nabla \cdot \boldsymbol{\omega}' = 0$. The solenoidality of the average field is important in order to describe the geometry of coherent vortex structures. The instantaneous and fluctuating fields are expected to have streamlines and vortex lines that are quite random. Streamlines and vortex lines of the phase averaged field, however, are expected to be well-behaved, allowing results from different planes to be connected. The analysis of the phase averaged field, then, can help to understand the underlying physical processes in the flow and the coherent vortex topology.

Since there is cycle-to-cycle variation in the period of the pressure or velocity fluctuations, a continuous wavelet transform (CWT) was used in order to determine the instantaneous phase of the shedding cycle. The CWT using a complex valued wavelet allows one to determine the instantaneous phase of fluctuations within a signal at the various scales (frequencies) contained within the signal. The CWT of a velocity signal, $u(t)$, with scale λ (proportional to the inverse of frequency) and time lag τ, is defined as

$$W(\lambda,\tau) = \int_{-\infty}^{\infty} u(t)\psi^*_{\lambda,\tau}(t)dt \tag{3}$$

where the asterisk denotes the complex conjugate of the wavelet function, $\psi_{\lambda,\tau}(t)$—a function with compact support that is stretched or shifted in time by changing the scale and lag constants λ and τ—where

$$\psi_{\lambda,\tau}(t) = \frac{1}{\sqrt{\lambda}}\psi\left(\frac{t-\tau}{\lambda}\right) \tag{4}$$

The analyzing wavelet used is the complex Morlet wavelet, shown in Fig. 4. It is constructed from a harmonic oscillation with an amplitude that has an envelope with the shape of a Gaussian function. The Morlet wavelet with bandwidth, f_b, and center frequency, f_c, is defined as

$$\psi(t) = \frac{1}{\sqrt{\pi f_b}} e^{i2\pi f_c t} e^{-t^2/f_b} \tag{5}$$

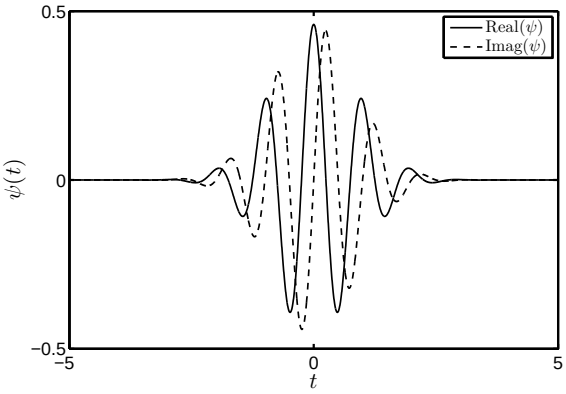

FIGURE 4: THE COMPLEX MORLET WAVELET.

The vortex shedding cycle can be analyzed by taking the complex value of the wavelet transform at the scale associated with the frequency of vortex shedding (corresponding to the peak frequency of the Fourier power spectra). The phase angle of the wavelet transform at any instant in time, then, is obtained by taking the arctangent of the complex coefficient, $\phi = \tan^{-1}\Im(W)/\Re(W)$. The mother wavelet (which is the basic wavelet which is subsequently scaled and shifted in time) used had $f_b = 1.5$ Hz and $f_c = 1$ Hz. In order to analyse the phase of the vortex shedding process, the Mother wavelet is scaled to have a center frequency equal to the frequency peak in the Fourier power spectra and the convolution integral of Eq. (3) is taken. An example of the phase determination with the CWT of a velocity measurement is shown in Fig. 5.

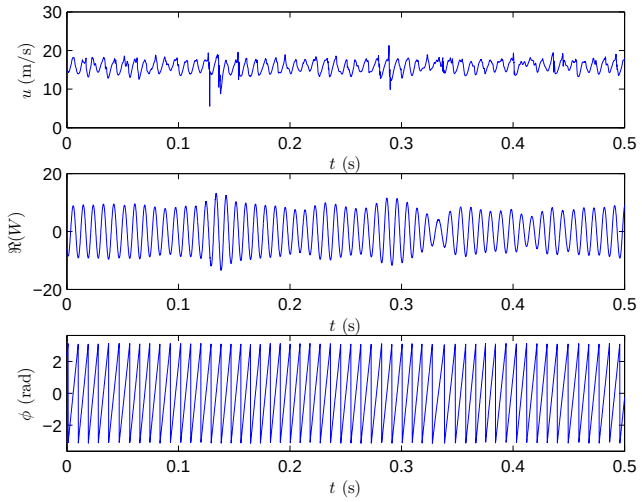

FIGURE 5: EXAMPLE OF PHASE DETERMINATION METHODOLOGY. A HOT-WIRE VELOCITY SIGNAL (TOP), THE REAL PART OF THE CWT AT THE VORTEX SHEDDING FREQUENCY (MIDDLE), AND THE PHASE (BOTTOM) ARE SHOWN. THE HOT-WIRE MEASUREMENT SHOWN WAS COLLECTED AT $x/d = 3$, $y/d = 2$, AND $z/h = 0.5$ FOR A $h/d = 4$ SQUARE-CROSS-SECTION CYLINDER.

4 RESULTS AND DISCUSSION

To elucidate the three-dimensional topology of the periodically shed structures, the spatial distribution of the phase relation is first considered, followed by phase-averaged velocity field results.

The reason that the relative phase field can elucidate the wake flow itself is because the velocity, pressure, and vorticity fluctuations at a point are caused by nearby passing vortices. Within a plane tangent to convecting vortices (for example, a vertical-streamwise plane which at least initially contains the vortices generated within the vertical shear layers), iso-contours of the phase of the velocity fluctuations will be parallel at some instant to the phase averaged vortex cores in the wake. By the Biot-Savart law, the velocity fluctuations will be an integrated effect of all of the vorticity in the flow. The assumption behind interpreting the iso-contours of constant phase as being aligned with vortices is that the phase of the fluctuation intensity is being governed by primarily the nearest vortex, and the integrated effect of other vortices is negligible. At points further removed from vortex cores, or in planes not tangent to vortex cores, the phase cannot be interpreted in this way, but may still yield information on the process.

Measurements have been taken with a fixed hot wire on one side of the wake while a rake of three hot wires (mounted vertically) has been traversed over planes at $y/d = -1.1$ and $y/d = -2$ at two free-stream velocities ($U_\infty = 8$ m/s and 15 m/s). The first hot wire (mounted at $x/d = 0.5$, $y/d = 1.1$, $z/h = 0.5$), is used as a phase reference, $\phi_R(t)$, for the vortex shedding process. The average relative phases to the fixed reference wire, $\Delta\phi = \phi(t) - \phi_R(t)$, measured and iso-contours of the relative phases are shown for square-cross-section cylinders in Figs. 6, 7, and 8. Similarly, results for circular-cross-section cylinders are shown in Figs. 9 and 10. Generally, the Reynolds number effect is small in the average phase measurements with the exception of perhaps a slight change in the formation length or a slightly different acceleration of the vortices.

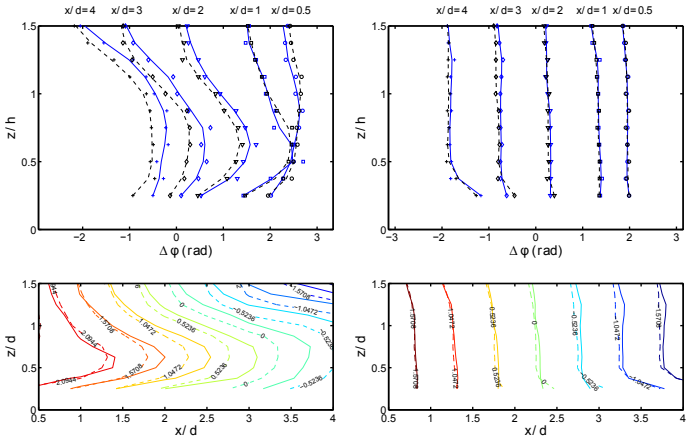

FIGURE 6: ASPECT RATIO $h/d = 1$ SQUARE-CROSS-SECTION CYLINDER RELATIVE PHASE (TOP) AND ISO-CONTOURS OF RELATIVE PHASE (BOTTOM). DATA COLLECTED AT $U_\infty = 8$ m/s (SOLID LINE) AND $U_\infty = 15$ m/s (DASHED LINE); $y/d = -1.1$ (LEFT) AND $y/d = -2$ (RIGHT).

A shared attribute of all results is that periodic fluctuations at points towards the free end lag those at points closer to the plate. This leads in the vicinity of the free end to iso-contours of the phase, and thus (by the assumptions stated above), the vortices, to be inclined backwards (upstream) towards the obstacle, giving rise to streamwise vorticity. Nearer to the plate, at the lowest measurement points ($z/h = 0.25$) the vortex lines tend to be more upright (vertical) without the obliqueness observed towards the tip. The exception to the upright lines of constant phase is the cube, where the iso-contours of the phase tend to incline back toward the obstacle at points close to both the free end and towards the plate. This obliqueness near the plate presumably indicates again the development of streamwise vorticity in the vicinity of the plate. Other obstacles may in fact show a

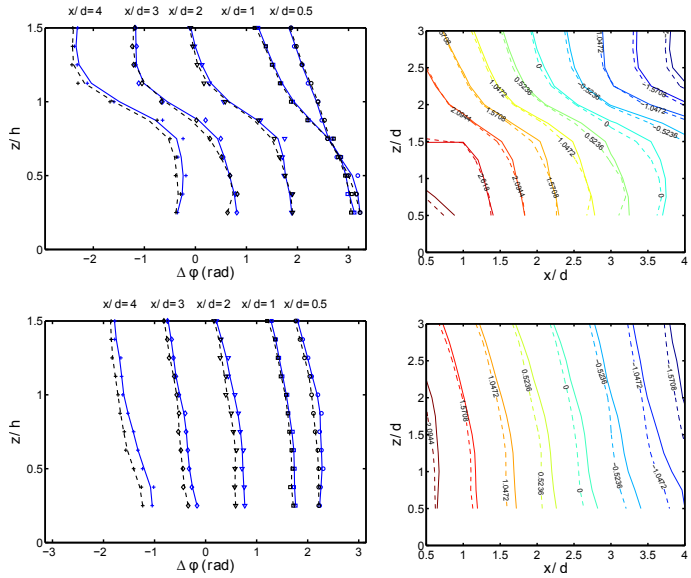

FIGURE 7: ASPECT RATIO $h/d = 2$ SQUARE-CROSS-SECTION CYLINDER RELATIVE PHASE (LEFT) AND ISO-CONTOURS OF RELATIVE PHASE (RIGHT). DATA COLLECTED AT $U_\infty = 8$ m/s (SOLID LINE) AND $U_\infty = 15$ m/s (DASHED LINE); $y/d = -1.1$ (TOP) AND $y/d = -2$ (BOTTOM).

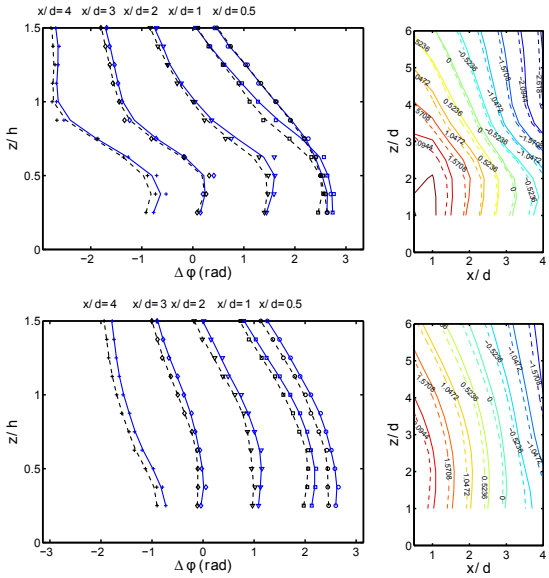

FIGURE 8: ASPECT RATIO $h/d = 4$ SQUARE-CROSS-SECTION CYLINDER RELATIVE PHASE (LEFT) AND ISO-CONTOURS OF RELATIVE PHASE (RIGHT). DATA COLLECTED AT $U_\infty = 8$ m/s (SOLID LINE) AND $U_\infty = 15$ m/s (DASHED LINE); $y/d = -1.1$ (TOP) AND $y/d = -2$ (BOTTOM).

similar tendency closer to the plate, but that is not clear from the present measurements because hot-wire anemometers could not be positioned closer to the plate surface. The no-slip condition at the wall may be enough to explain streamwise reorientation of the initially vertical vortices close to the plate surface. However, the same cannot be said for the vorticity towards the free end.

The measurements at $y/d = -2$ are further from vortex cores and tend to show more far-field effects of the vorticity fluctuations as vortices are being convected. At $y/d = -1.1$, however, it is much clearer where the top of the wake is (corresponding approximately to the section of high phase gradients). Above this high phase gradient region, the velocity fluctuation intensity is much lower than it is for points closer to the plate. For the circular cylinders, the high phase gradient region—which is interpreted as the inclination at the top of the shed vortices—seems to be much lower along the obstacle (consistent with the statement by Kawamura et al. [7] that vortex shedding is suppressed toward the free end of circular cylinders). The square cylinder vortices, however, seem to span the entire height (albeit toward the free end they lack a predominantly vertical vortex structure by somewhere between $z = 0.5h$ and $z = h$), and in the case of the cube, vortices may perhaps extend even above the obstacle height. For these lowest aspect ratio obstacles, it is clear that the inclination of vortices is an increasingly more dominant feature of the wake.

The authors have recently described in Ref. [8] a Navier-Stokes simulation of a $Re = 500$ flow over an aspect ratio $h/d = 2$ surface-mounted square cylinder immersed in a thin laminar boundary layer. Visualizing vortex cores using the method of Jeong and Hussain [9], a similar tendency for vortices to be inclined back towards the obstacle was observed in the vicinity of the free end of the obstacle. The manifestation of streamwise vorticity found in the mean field was described as being an outcome of Biot-Savart induction at the intersection of fluid layers containing predominently vertical and lateral oriented vorticity generated by pressure gradients along the obstacle side faces and tip (of which the layer of concentrated vorticity can be conceptually treated as two initially orthogonal vortex sheets). This provides a mechanism for the generation of the experimentally observed streamwise vorticity. This mechanism leads to the vortices bending back upstream near the obstacle tip and is expected to be important in any free-shear flow with curvature or sharp junctions of adjacent shear layers (notably also square or rectangular jets), and is present for the entire range of finite bluff cylinders studied.

Such phase measurements start building a picture of the vortex lines in the wake. A typical vortex line just downstream of the obstacle is shown in the top left corner of Fig. 11. The vorticity vector is aligned along the shear layers. Near to the plate,

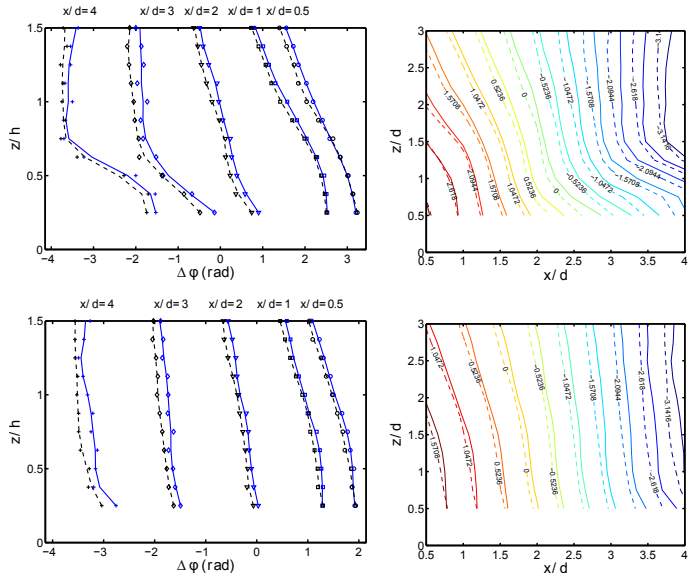

FIGURE 9: ASPECT RATIO $h/d = 2$ CIRCULAR-CROSS-SECTION CYLINDER RELATIVE PHASE (LEFT) AND ISO-CONTOURS OF RELATIVE PHASE (RIGHT). DATA COLLECTED AT $U_\infty = 8$ m/s (SOLID LINE) AND $U_\infty = 15$ m/s (DASHED LINE); $y/d = -1.1$ (TOP) AND $y/d = -2$ (BOTTOM).

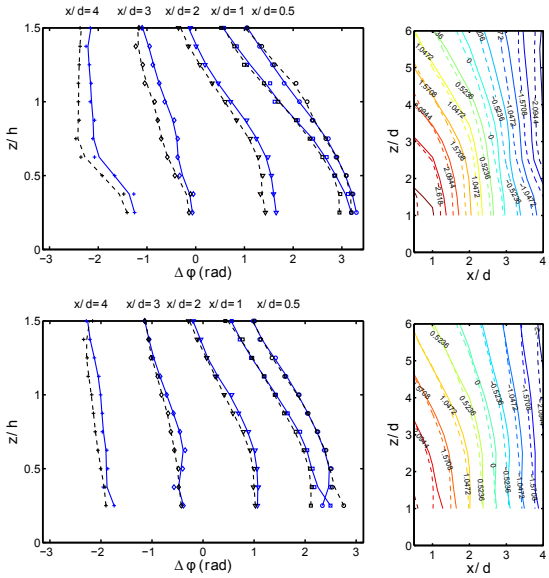

FIGURE 10: ASPECT RATIO $h/d = 4$ CIRCULAR-CROSS-SECTION CYLINDER RELATIVE PHASE (LEFT) AND ISO-CONTOURS OF RELATIVE PHASE (RIGHT). DATA COLLECTED AT $U_\infty = 8$ m/s (SOLID LINE) AND $U_\infty = 15$ m/s (DASHED LINE); $y/d = -1.1$ (TOP) AND $y/d = -2$ (BOTTOM).

the vortex lines run tangent to the surface in the lateral direction within the boundary layer. The vortex line arches up within the separated shear layers from the side faces, and is connected over the top within the tip shear layer. Such a characteristic vortex line would be expected in the time averaged field. In the phase averaged field, however, the vortex lines behave dynamically according to primarily two mechanisms. Both are easily described in terms of Biot-Savart induction.

The more obvious mechanism concentrating vortex lines is that shown in Fig. 11(b). This is the mechanism that governs von Kármán-type shedding which is ubiquitous in separated bluff body wakes. Vortex lines are found to concentrate themselves when a vortex sheet is perturbed by the Kelvin-Helmholtz instability which causes the vortex sheet to roll-up by an induction mechanism that becomes increasingly strong as the vortex sheet is deformed. The vortices formed through the concentration of vortex lines on opposing sides of the wake then interact with one another to determine the subsequent development of the wake. This mechanism is by its nature two dimensional.

The three-dimensionality of the finite bluff body wake arises by interaction of this two-dimensional mechanism with the second mechanism, shown in Fig. 11(a), by which the rolled-up vortices along the height of the obstacle are subsequently bent backwards by the added induction of the tip shear layer.

To describe this mechanism, we take the Helmholtz decomposition of the velocity field $\mathbf{u} = \mathbf{u}^{(\omega)} + \mathbf{u}^{(\phi)}$ where $\mathbf{u}^{(\omega)}$ and $\mathbf{u}^{(\phi)}$ are rotational and potential vector fields. The rotational part of the velocity field, $\mathbf{u}^{(\omega)}$, is that induced by the vorticity field and is obtained from the Biot-Savart law:

$$\mathbf{u}^{(\omega)} = \frac{1}{4\pi} \int \frac{\boldsymbol{\omega} \times \mathbf{r}}{r^3} dV \tag{6}$$

Consider the concentrated vorticity of one of the shear layers, shown in Fig. 12, generated along the height, $\overline{AB}$: the primary source of induced velocity of point A is caused by the nearby ω_y vorticity at a point E. The induced velocity is in the opposite direction to the main flow direction, and thus causes a lag of the vortices relative to the free-stream velocity. The induced velocity, due to the proximity of the tip vortices, will be stronger at A than the induced velocity felt at the midpoint of $\overline{AB}$, and hence as the flow convects, the extremity A will move at a slower rate, deforming any initially straight vortex lines. The same argument can be made of point C caused by the ω_y vorticity at F, and likewise with the effect of the ω_z vorticity inducing a backward directed induced velocity at the extremities of the tip vortex structure $\overline{EF}$. Some negative induced velocity by these

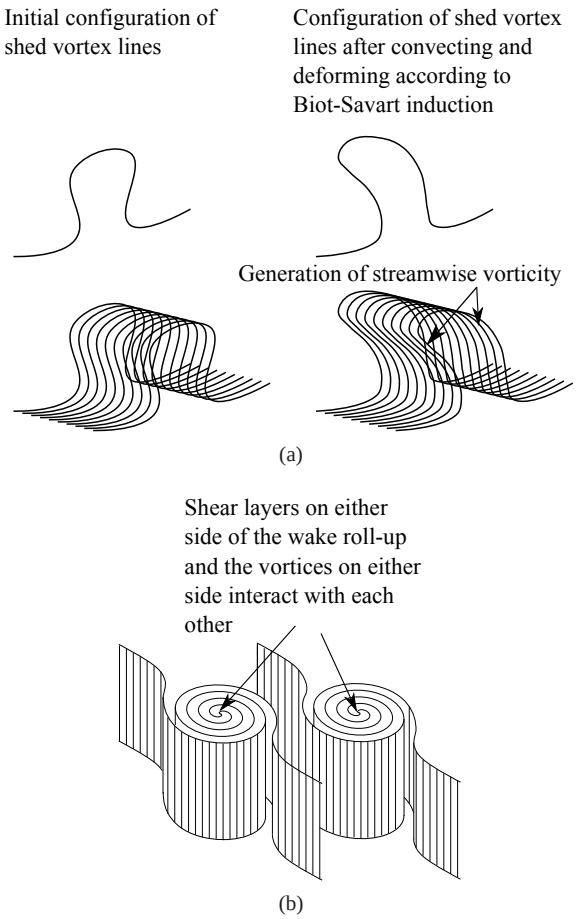

FIGURE 11: PREVALENT PHYSICAL MECHANISMS CONCENTRATING VORTICITY IN THE WAKE (a) BACKWARD INCLINATION OF VORTEX LINES GIVING RISE TO STREAMWISE VORTICITY; (b) VORTEX ROLL-UP AND SUBSEQUENT LATERAL INTERACTION WITH OPPOSITE ROLLED-UP VORTEX.

vortices will also be felt by points B and D, however, the more important vorticity for these points will be the boundary layer vorticity which will enforce the no-slip condition at the wall, and hence will restrain most movement of these points. The result is that all extremities of these regions of concentrated vorticity A through F will show a reduced convection velocity, and streamwise vorticity will arise in the wake due to re-orientation and stretching of the legs of these vortices.

If vortices generated in the tip are disconnected from vortices along the height of the cylinder, these may themselves bend backwards and may cause another set of streamwise vortices counter-rotating with the bent back vortices from the side-wall shear layers, as seen in [8]. The roll-up mechanism of the tip, however, is purely a Kelvin-Helmholtz instability, and no set of counter-rotating vortices is generated to interact with the tip vortices. It is unlikely, then, that if lateral tip vortices are independent of the vertical vortices (i.e. not connected with the vertical vortices as a single structure) that they will be seen as vortex cores (identified by a method such as described by [9]) in the phase averaged field.

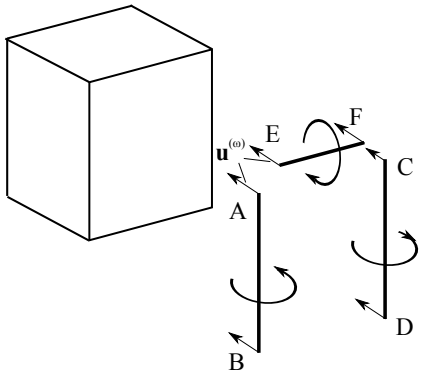

FIGURE 12: BIOT-SAVART INDUCED VELOCITY ON LINES OF CONCENTRATED VORTICITY WITHIN THE OBSTACLE SHEAR LAYERS.

The changes in the induced velocity at different points along the shed structure adequately explain the mechanism leading to the inclination of the shed structures. It is observed that downstream of the formation region, the convective velocity, U_c (the resulting streamwise velocity component of the vortex core when superimposing the potential and the induced rotational velocity fields), does not vary along the height. Hence, the structure bends until the induced velocity finds an equilibrium and the structure convects as one at the speed U_c.

As a part of a larger investigation into the three-dimensional structure of finite bluff body wakes, PIV measurements on a $h/d = 4$ square-cross-section cylinder have also been conducted. These measurements can be used to confirm the interpretations from the hot-wire phase calculations and can give further insights into the wake field.

As with the hot wires, it is necessary to have a fixed phase reference in order to reconstruct the three-dimensional field and to conduct phase averaging. PIV requires seeding particles, and for this reason, measurements made by fragile hot-wire anemometers could not be used as a fixed phase reference. In order to conduct phase resolved PIV measurements, then, surface pressure measurements were taken and used as a phase reference. Measurements of the surface pressure were taken at $0.25h$ where the fluctuation amlitude is typically very high.

Figure 13 shows phase averaged velocity measurements in the convective reference frame, where the velocity vector is given

by $\mathbf{u}-\mathbf{U}_c$, where $\mathbf{U}_c = 0.75U_\infty$, as per Fig. 2. Figure 14 shows colour contours of the vertical component of vorticity, ω_z and the solid black line denotes the bounding line of regions $\lambda_2 < 0$ which define vortex cores in the sense described by [9]. λ_2 is the second eigenvalue (if the eigenvalues are ordered from smallest to largest) of the tensor $S_{ij}S_{jk}+\Omega_{ij}\Omega_{jk}$ with $S_{ij} = 1/2(u_{i,j}+u_{j,i})$ and $\Omega_{ij} = 1/2(u_{i,j}-u_{j,i})$ the strain rate and rotation tensors, respectively. λ_2 had to be calculated two-dimensionally (neglecting velocity and velocity gradients in the z-direction) as the PIV measurements are planar. Calculating λ_2 in this way is valid in regions where the vorticity is primarily vertical (oriented along z), and vertical velocity gradients are small. Towards the tip, it is clear that these assumptions break down. Looking at vortex cores determined by a two-dimensional λ_2 under such circumstances is not, however, without precedent in the experimental literature as the definition will pick up any portion of a vortex core that still has significant vorticity normal to the plane of measurement.

The negative circulation vortex that has just been shed displayed in Fig. 14 (denoted structure A), tends to show a λ_2 contour that is seen further and further back toward the obstacle at higher locations, indicating an inclination of the structure. It can also be seen that at $0.75h$, the λ_2 contour disappears at around $5d$, indicating that the vortex has either been reoriented to the streamwise or lateral directions or has been convected downwards out of the plane. At $0.5h$, interestingly the λ_2 defined vortex core initially rolls-up close to the obstacle but has subsequently split into two by approximately $7d$. At $0.25h$, this splitting of the core tends to be observed even further along the streamwise coordinate. This splitting of a vortex structure into two vortices with the same rotational sense is initially quite surprising. In fact, the observed split of the vortex structure suggests the formation of a vortex strand connecting to the initial vertically oriented vortex on the opposing side of the wake. These connectors can provide a topologically consistent, three-dimensional mechanism for satisfying the solenoidal condition on the vorticity field while preserving the spatially periodic structure of the system of shed vortices. This hypothesis is currently being investigated.

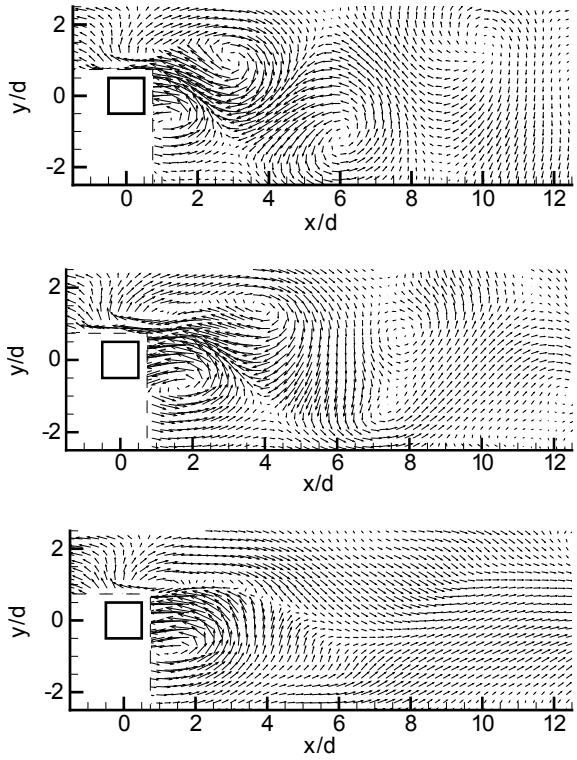

FIGURE 13: PHASE AVERAGED CONVECTIVE FRAME VELOCITY VECTORS, $\mathbf{u}-\mathbf{U}_c$, AT $0.25h$, $0.5h$, AND $0.75h$ (FROM TOP TO BOTTOM). BLANKED AREA IS IN THE SHADOW OR REFLECTION OF THE LASER LIGHT SHEET. ALL THREE MEASUREMENTS ARE TAKEN FOR A COMMON RELATIVE PHASE OF $\phi = 1.1$ RELATIVE TO THE SURFACE PRESSURE FLUCTUATIONS.

5 CONCLUDING REMARKS

The near-wake vorticity dynamics are fundamentally an interplay between the physical mechanisms: (*i*) shear layer roll-up on either side of the wake and subsequent cross-stream interaction of the two shear layers and (*ii*) the backward reorientation of vortices toward the free end of the obstacle—consistent with a higher backward Biot-Savart induced velocity from the vorticity contained within the three shear layers in the initial formation region. A third mechanism may also be important in all cases, but has primarily been seen in the relative phase results of the $h/d = 1$ square-cross-section cylinder, (iii) the no-slip condition which again reorients vorticity by lowering the convective velocity of the near-wall portions of vortex lines. The concentration of vortex lines by these mechanisms, and the predominant effects of rotation over shear on fluid elements leads to the production of vortices. It is clear from the measurements shown that indeed we have a lean-back mechanism of the vortices in the wake of the finite obstacles that is increasingly important as the aspect ratio, h/d is reduced, and is an effect of stronger importance in square- as compared to circular-cross-section wakes. In fact, the vortices in the wake do not seem to extend to the same height as in the square-cross-section wake, and thus the effect of the tip shear layer is reduced.

Whether the vertical vortices are connected across the tip shear layer or whether they are merely bent back toward the obstacle at the free end cannot yet be assessed conclusively. Although by solenoidality, vortex lines in the wake are quite certainly connected across the wake in this way as a result of the direction of the vorticity vector and the solenoidality of the vorticity field, a vortex (as defined by a method such as that of [9]) may end as rotation and shear components of the fluid deforma-

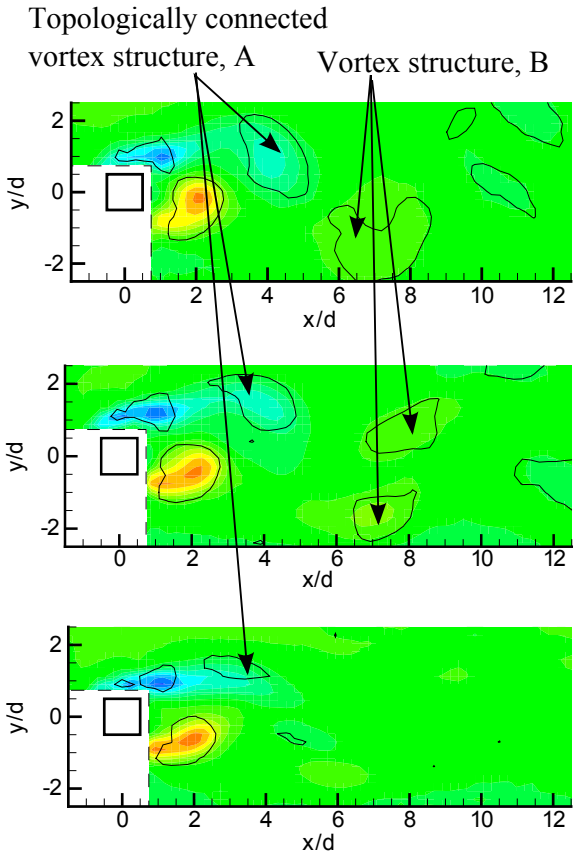

FIGURE 14: VORTICITY CONTOURS WITH LINES OF $\lambda_2 = 0$ OF PHASE AVERAGED MEASUREMENTS AT $0.25h$, $0.5h$, AND $0.75h$ (FROM TOP TO BOTTOM). CONTOUR INCREMENTS ARE $0.4U_\infty/d$. BLANKED AREA IS IN THE SHADOW OR REFLECTION OF THE LASER LIGHT SHEET. ALL THREE MEASUREMENTS ARE TAKEN FOR A COMMON RELATIVE PHASE OF $\phi = 1.1$ RELATIVE TO THE SURFACE PRESSURE FLUCTUATIONS.

tion change throughout the field. In fact, the vortex structure toward the free end of the obstacle may be even more complex at the tip than expected. The phase averaged PIV measurements seem to indicate that vortices (as identified by a λ_2 based only upon the x and y deformation components) tend to split, suggesting a vortex strand connecting the initial vertically oriented vortex on the opposing side of the wake perhaps also accounts for the observed downwash seen in the mean flow symmetry plane. Further measurements are being carried out to develop further insight into the vortex sturcture of the free end side of the wake. Further questions about the wake vortex structure, such as the symmetry and anti-symmetry of shed vortices will be tackled in an upcoming publication by the authors.

ACKNOWLEDGMENT

The authors extend their gratitude to the Natural Sciences and Engineering Research Council of Canada and Alberta Innovates Technology Futures for their financial support of this work.

REFERENCES

[1] Sakamoto, H., and Arie, M., 1983. "Vortex shedding from a rectangular prism and a circular cylinder placed vertically in a turbulent boudary layer". *J. Fluid Mech.,* ***126***, pp. 147–165.

[2] Wang, H. F., Zhou, Y., Chan, C. K., and Lam, K. S., 2009. "Momentum and heat transport in a finite-length cylinder wake". *Exp. Fluids,* ***46***, pp. 1173–1185.

[3] Etzold, F., and Fiedler, H., 1976. "Near-wake structure of a cantilevered cylinder in a cross-flow". *Z. Flugwiss.,* ***24***(2), pp. 77–82.

[4] Adaramola, M., Akinlade, O., Sumner, D., Bergstrom, D., and Schenstead, A., 2006. "Turbulent wake of a finite circular cylinder of small aspect ratio". *J. Fluids and Structures,* ***22***, pp. 919–928.

[5] Mason, P. J., and Morton, B. R., 1987. "Trailing vortices in the wakes of surface-mounted obstacles". *J. Fluid Mech.,* ***175***, pp. 247–293.

[6] Wang, H. F., Zhou, Y., Chan, C. K., Wong, W. O., and Lam, K. S., 2004. "Flow structure around a finite-length square prism". *15th Australasian Fluid Mechanics Conference*.

[7] Kawamura, T., Hiwada, M., Hibino, T., Mabuchi, I., and Kumada, M., 1984. "Flow around a finite circular cylinder on a flat plate. cylinder height greater than turbulent boundary layer thickness". *Bulletin of the JSME,* ***27***(232), pp. 2142–2151.

[8] Bourgeois, J. A., Sattari, P., and Martinuzzi, R. J., 2010. "Development of streamwise vortex structure in the wake of a finite surface mounted square cylinder". *CFD Society of Canada 18th annual conference*.

[9] Jeong, J., and Hussain, F., 1995. "On the identification of a vortex". *J. Fluid Mech.,* ***285***, pp. 69–94.